Surfing the High Energy Output Branch of Nonlinear Energy Harvesters

D. Mallick,[1] A. Amann,[1,2] and S. Roy[1,*]
[1]Tyndall National Institute, Lee Maltings, Dyke Parade, Cork T12 R5CP, Ireland
[2]School of Mathematical Sciences, University College Cork, Cork T12 XF62, Ireland
(Received 18 March 2016; revised manuscript received 12 June 2016; published 4 November 2016)

Hysteresis and multistability are fundamental phenomena of driven nonlinear oscillators, which, however, restrict many applications such as mechanical energy harvesting. We introduce an electrical control mechanism to switch from the low to the high energy output branch of a nonlinear energy harvester by exploiting the strong interplay between its electrical and mechanical degrees of freedom. This method improves the energy conversion efficiency over a wide bandwidth in a frequency-amplitude-varying environment using only a small energy budget. The underlying effect is independent of the device scale and the transduction method and is explained using a modified Duffing oscillator model.

DOI: 10.1103/PhysRevLett.117.197701

Recently, scavenging electrical energy from environmental vibration using miniaturized systems has received enormous attention due to its potential to provide an alternative energy solution for wireless sensor nodes leading to the vision of the Internet of Things. The vibrational energy harvesters (VEHs) have emerged over the years as an attractive solution, as they will not only eliminate the required maintenance cost and chemical hazards associated with batteries but also expand the life span of the power supply. Most of the earlier reported VEHs are linear [1–5] and have the limitation of a narrow bandwidth. *Nonlinear-oscillator*-based energy harvesters improve the off-resonance performance significantly due to their inherent wideband frequency response. Various nonlinear energy harvesters with different types of potential energy functions, e.g. single-well [6–10], double-well [11–15], and triple-well [16–18] systems, have been explored comprehensively to achieve energy transduction over a wide frequency range. However, it has been observed that the branching of the frequency response introduces the phenomena of multistability and hysteresis in the dynamics of the devices [8,9,19], which means that a number of stable steady states with different energy outputs may coexist. The device selects a stationary state depending upon the frequency schedule of the external excitation and the initial conditions [19,20].

In general, many dissipative nonlinear dynamical systems exhibit the coexistence of several stable states for a given set of parameters and can be found in various disciplines of science, including electronics [21], optics [22], mechanics [23], and biology [24]. In such systems, the control of the coexisting states is critical, because the corresponding attractors are extremely sensitive to any sort of perturbation. A number of control mechanisms [25] have been reported by researchers to achieve the desired state in a multistable system such as feedback control [26], using chaotic [27] or noise [28] signals or by creating a crisis of the undesired state [29].

The vibrational energy harvesting application, which is a crossover between mechanical and electrical domains, serves as the proving ground for many nonlinear dynamical phenomena. In principle, it is desirable to *surf* the state with the largest possible energy output. However, in a real-world environment there is little control available over the frequency and amplitude of the driving vibration, and therefore a large energy output is not guaranteed. Thus, efficient and convenient control mechanisms are required to perturb the system from the low energy branches (LEBs) to the high energy branch (HEB) to facilitate the maximum energy conversion within the region of multistability. Previously, this pertinent problem was addressed by Cammarano *et al.*, who proposed the concept of altering the natural frequency of the oscillator to a higher value where only a single solution exists for the given excitation frequency and then reducing the natural frequency as the oscillator response stays on the HEB [30]. This concept is similar to the formation of a crisis, but the destruction of coexisting states can be difficult for some nonlinear systems, as small perturbations of the system parameters can give rise to new complex multistabilities. Zhou *et al.* used mechanical impact to provide additional kinetic energy to the oscillator to obtain the HEB [31]. Both of these mechanisms involve mechanical modifications which are practically not very convenient. Recently, Masuda and Sato introduced an electrical method to destabilize the lower output branch by developing a switching circuit of the load resistance between positive and negative values depending on the response amplitude of the oscillator [32]. This switching of the effective damping is difficult to implement and changes the dynamics of the oscillator, which is not desirable.

In this Letter, we demonstrate that a suitable electrical control signal switches the state of a nonlinear VEH from the LEB to the HEB. The VEHs have an inherent connection between their mechanical and electrical degrees

of freedom. We exploit this interplay and supply a periodic electrical signal over a short period of time to the system to initiate the large amplitude mechanical motion when the system response is in the LEB. The dynamical characteristics of the proposed methods are theoretically reproduced and explained by a modified Duffing oscillator model. We expect this elegant approach can be generalized to systems of any scale (MEMS or nanoscale devices) and with different transduction mechanisms where the manipulation of mechanical parameters may not be easy to implement.

Experimentally, we have demonstrated the proposed scheme using a stretching-strain-induced nonlinear electromagnetic energy harvester [Fig. 1(a)]. The hardening nonlinearity is induced in the harvester through the large amplitude stretching strain in the fixed-guided spring arms. The wideband response of the system occurs due to the stretching-induced, amplitude-dependent spring stiffness [9]. The proposed switching scheme is shown in a circuital form in Fig. 1(b), where the harvester is modeled using a spring-mass-damper system. A voltage $\gamma\dot{x}$ is induced in the coil (internal resistance R_C) of the EM harvester, where γ is the electromagnetic coupling coefficient and $\dot{x}$ is the velocity of the mechanical oscillator. The electrical power is extracted through the load resistance R_L, which is connected in series with the coil. Additionally, a voltage source V_A (with internal resistance R_A) is connected across the coil, which generates electrical voltage over a short period of time to supply enough energy to perturb the system to switch the state when needed.

The frequency response widens with increasing accelerations [subplot in Fig. 2(a)], as the jump-down frequency during the up sweep gradually increases. During the down sweep, the VEH follows the LEB of the hysteresis, resulting in a very small output power. In Fig. 2(a), we demonstrate the switch from the LEB to the HEB for a mechanical driving frequency $f_m = 70$ Hz, at an acceleration of $0.5g$. We supply a periodic sinusoidal electrical signal of frequency $f_A = 70$ Hz and 5 V amplitude within the time interval from 20 to 20.2 s, which is approximately 15 cycles. As a consequence, the peak output power changes dramatically by a factor of more than 35, from the LEB steady state value of 16 μW before the switching period to the HEB steady state value of 563 μW after the switching period. This large power is maintained even without any further supply of electrical energy. This transition from the LEB to the HEB is indicated by the arrow shown in the subplot in Fig. 2(a). The experimental result is validated using numerical simulations based on a modified Duffing oscillator [Fig. 2(b)]. The equation of motion of the modified Duffing oscillator is derived based on the model shown in Fig. 1(b). The generated voltage V_A is given as

$$V_A(t) = \begin{cases} V_{OA}\sin(2\pi f_A t + \phi) & \text{for } t_i \le t \le t_f \\ 0 & \text{else,} \end{cases} \quad (1)$$

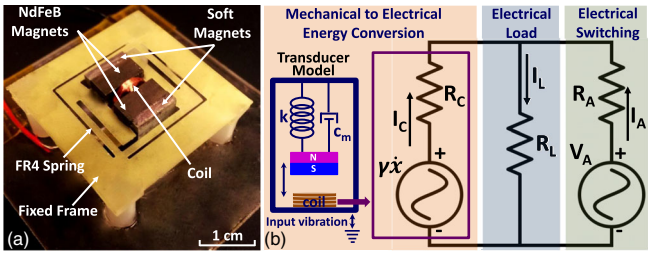

FIG. 1. Prototype and the proposed method. (a) The experimental prototype of the nonlinear EM harvester. (b) Proposed circuit to model the electrical actuation scheme. The mechanical to electrical energy conversion transducer consists of a spring-mass-damper system.

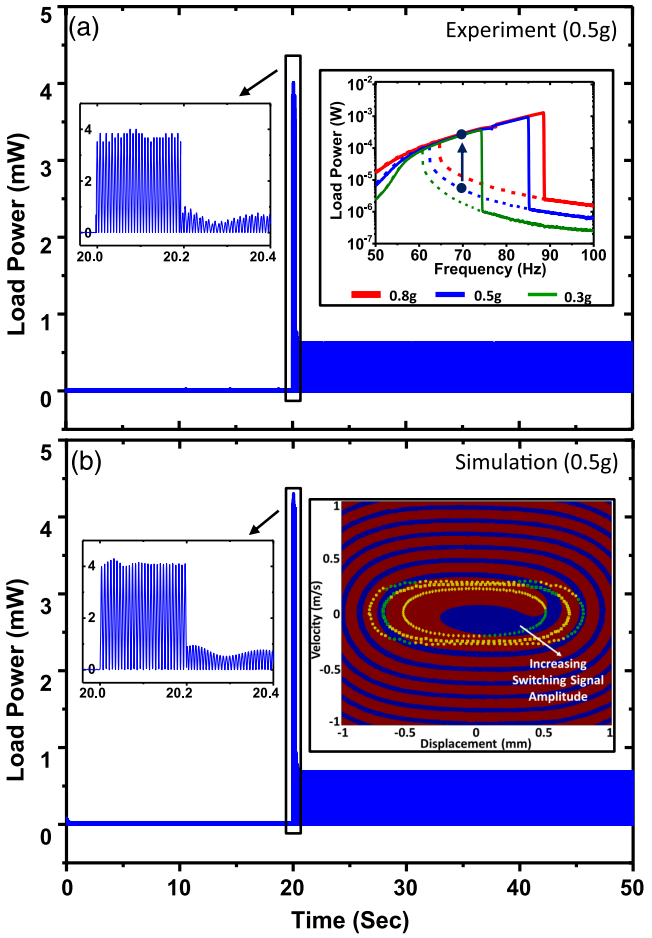

FIG. 2. Transition from the LEB to the HEB. (a) Experimental result. The subplot indicates the load power as a function of the input frequency under different input accelerations without any electrical switching. The up sweep is indicated by the solid line and the down sweep by the dotted line. (b) Numerical result. The basin of attraction of the nonlinear oscillator is shown. High and low energy attractors are denoted by red and blue regions, respectively. Successful (yellow) and unsuccessful (green) switching are mapped in to the basin of attraction for varying the phase of the switching signal at fixed amplitudes (diamonds, 5 V; squares, 15 V; circles, 25 V).

where V_{OA}, f_A, and ϕ are the amplitude, frequency, and phase, respectively, of the signal within the switching period and t_i and t_f are the starting and ending time of the switching period, respectively. V_A drives a large current (I_A) through the coil which, in turn, produces a magnetic field that forces the outer magnetics along with the resonating spring to vibrate with a large amplitude. Using Kirchhoff's law for the loops in Fig. 1(b), the net current I_C through the coil is given as

$$I_C(\dot{x},t) = I_L - I_A = \frac{\gamma\dot{x}}{R_C} - \frac{R_L}{R_C}\frac{V_A(t)R_C + \gamma\dot{x}R_A}{R_CR_A + R_AR_L + R_LR_C}. \tag{2}$$

Taking into account the effect of the additional voltage signal, the coupled electromechanical equation of motion of the oscillator is given as

$$m\ddot{x} + 2c_m\dot{x} + kx + k_nx^3 + \gamma I_C = -m\ddot{z}, \tag{3}$$

where m, c_m, k, and k_n denote the mass, mechanical damping coefficient, linear spring constant, and cubic spring constant of the VEH, respectively. z is the displacement amplitude of the external vibration. Equation (3) has been numerically solved using the Runge-Kutta method and compared with the experimental results.

The switching action attributes to the basin of attraction of the oscillator as indicated in the subplot in Fig. 2(b). The basin of attraction shows that, starting from different initial conditions at a vanishing driving force, the solution approaches either the LEB (blue) or the HEB (red). The state of the Duffing oscillator can be switched easily under external perturbation due to the intermingled nature of the basin of attraction, as the system can be driven from the current to the other attractor using a small amount of energy. We use this feature of the Duffing oscillator to intentionally perturb the system to the HEB. Previously, it has been demonstrated using basin of attraction plots that the steady states are largely dependent on the initial conditions and the phase space volume associated with the HEB shrinks as the system comes close to the jump-down frequency [9,19,33]. Close to the jump-up frequency, the phase space of the HEB is large, and comparatively small perturbations are sufficient to switch the state and vice versa. However, the phase ϕ of the switching signal relative to the mechanical driving force plays an important role in the switching action as illustrated by the yellow and green symbols in the basin of attraction plot in Fig. 2(b). By varying $\phi \in [0 \quad 2\pi]$ for fixed switching signal amplitudes, it is observed that even a very large switching amplitude cannot guarantee a successful switching. For a particular switching amplitude, the successful switching occurs for those phase values for which the oscillator lands in the high energy attractor just after the electrical signal is switched off and vice versa for the unsuccessful cases. In mathematical terms, the LEB and HEB correspond to stable fixed points in the Poincaré map of Eq. (3) with respect to the constant phase of the external driving force. The separatrix which divides the two basins of attraction is given by the stable manifold of the saddle of this Poincaré map.

To obtain further insight into the switching mechanism, we have mapped successful and unsuccessful switching for varying phases and amplitudes of the electrical switching signals [Fig. 3(a)]. For very small amplitudes, there is no switching as expected due to the lack of injected energy to facilitate a switch. For moderately high amplitudes, the probability of successful switching increases due to the presence of the high energy attractor near the origin. Thus, suitably injected electrical energy can relatively easily drive the oscillator from the low to the high energy attractor. Very high amplitude signals, on the other hand, can oscillate the system into concentric and shallow elliptical rings of high and low energy attractors. Therefore, the probability of switching decreases relatively as the unsuccessful switching is obtained for many phase values. The corresponding variation of the probability of switching is shown in Fig. 3(b). The optimization of the energy required for optimal control of coexisting states is, however, out of the scope of this Letter. The practical implication of this phase dependence of the switching method is to simply repeat the process if success is not obtained in the first attempt. Let E_0 be the energy required to apply the switching signal once and P_S be the probability of successful switching in one attempt. Then the total energy (E_T) that would be spent in order to switch the state is calculated as

$$E_T = P_SE_0\left(\sum_{k=1}^{\infty} k(1-P_S)^{k-1}\right) = \frac{E_0}{P_S}. \tag{4}$$

Since P_S is not too small, the total energy required is not very large under practical conditions even if successful switching into the HEB is not obtained in a single trial.

In general, there is no control over the amplitude and frequency of the ambient sources, and the convertible energy is distributed over broad ranges of these parameters, making nonlinear energy harvesters an attractive solution.

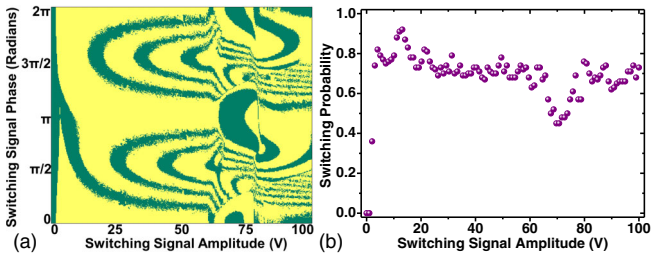

FIG. 3. Probabilistic study on the switching mechanism. (a) Mapping of successful (yellow) and unsuccessful (green) switching for varying the phase of the electrical switching signal with its amplitude. (b) Probability of successful switching as a function of the switching signal amplitude.

However, as mentioned already, the selection of the desirable branches in a nonlinear harvester is strongly dependent on knowledge of the input amplitude and frequency. Thus, its application is limited due to this fundamental effect without much effort to exploit it. Using our method, the oscillation can be sustained in the desired branch within the multistable regime. To demonstrate this improvement, we map two such input trajectories ($R \rightarrow R'$ and $S \rightarrow S'$) in Fig. 4 as both the above-mentioned parameters are varied simultaneously. The jump-up and jump-down lines correspond to saddle-node bifurcation lines of the Poincaré map and are plotted to define the multistate regime of the oscillation. Below $0.15g$, the two jump frequencies merge into a codimension-two cusp point at 57 Hz which is close to the linear resonance frequency of the device. The R to R' input variation is confined within the LEBs, defined by the area above the jump-down frequency line, and the hysteresis of the oscillation, whereas the input path S to S' crosses the threshold of the HEB regime, defined by the jump-up frequency line, before traversing back in the hysteresis again. The output response always remains in the LEB and HEB for input parameter values which are above the jump-down frequency line and below the jump-up frequency line, respectively. In the absence of the electrical actuation [Fig. 4(a)], the low amplitude oscillation is maintained as the oscillator enters the hysteresis region crossing the jump-down frequency line for both the input variation paths ($R1 \rightarrow R2$ and $S1 \rightarrow S2$). For S to S' trajectory, the oscillator is pushed to the HEB automatically when it crosses the jump-up frequency from the hysteresis region

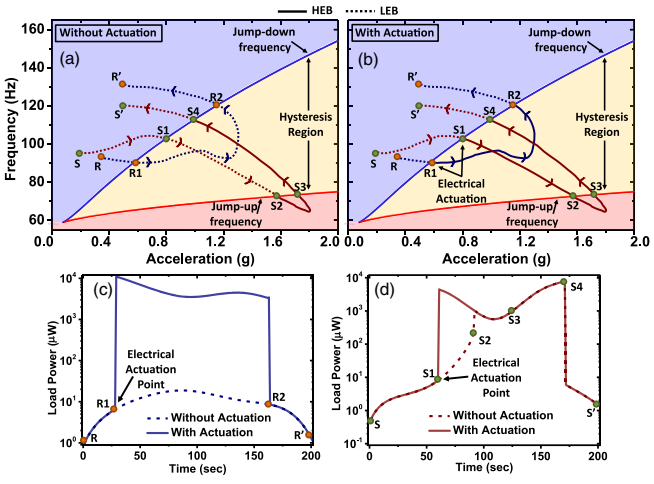

FIG. 4. Electrical switching under frequency-amplitude-varying input vibration. Two input vibration trajectories ($R \rightarrow R'$ and $S \rightarrow S'$) are defined. Jump-up and -down frequencies are plotted in (a) and (b) as a function of input acceleration using AUTO-07P [35]. Output states: (a) without the electrical actuation and (b) with the electrical actuation. Numerical results show the improvement in load power due to electrical actuation for input trajectories (c) $R \rightarrow R'$ and (d) $S \rightarrow S'$.

at $S2$ and remains there till $S3$, as that is the only available state. This high amplitude oscillation is continued even when the oscillator returns to the hysteresis from the HEB region through $S3$ and maintains the corresponding state until $S4$, as there are no other perturbations. By applying the short-duration electrical actuation at the inception of the hysteresis, the system can be driven onto the HEB, which persists during the entire multistate regime [Fig. 4(b)] for both the input vibrations. These result in substantial improvements in the harvesting efficiency over the entire trajectories (being more than 300 times for $R \rightarrow R'$), and the improvements are shown in Figs. 4(c) and 4(d), respectively, for the two input trajectories. The proposed method is significantly important for input excitations as R to R', where the device oscillates mostly within the multistable region. It is a classical approach in VEH applications to sweep either the frequency or acceleration of the input vibration which corresponds to straight lines parallel to either axis in Fig. 4(a) or 4(b). In such cases, the switching technique can be employed to surf the HEB during the down sweep (for frequency variation) or up sweep (for acceleration variation) (see Supplemental Material [34]).

One of the most significant concerns about the proposed approach is that a certain amount of energy needs to be supplied in order to facilitate the switching. However, this invested energy is quickly recovered through the increased power conversion in the HEB. This is demonstrated in Fig. 5, where the numerically calculated net electrical energy evolution of the system is shown. The net energy increases very slowly as long as the system remains in the LEB, as only a little power is generated. The energy is supplied electrically for 0.2 s, and this results in a negative slope of the energy curve. Once the system reaches the HEB, the slope of the energy curve becomes steep, as large power is generated. With a decreasing acceleration level, both the required switching energy and the energy recovery

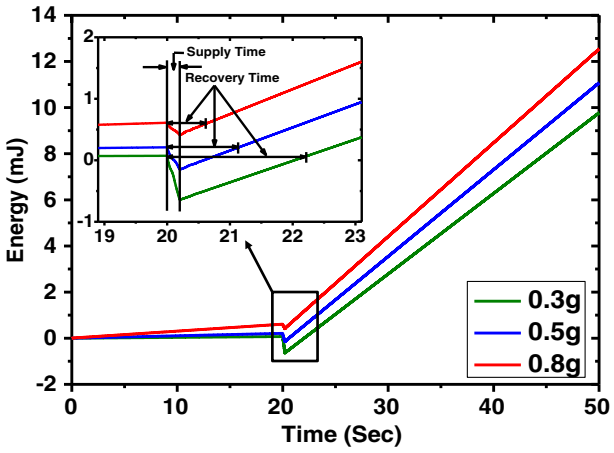

FIG. 5. The evolution of the net electrical energy under different acceleration levels. The negative slope from 20 to 20.2 s indicates that energy is supplied over that period of time.

time become larger. If the switching is successful at the first attempt, the externally supplied energy is recovered within 2 s at $0.3g$, which shortens to 0.4 s at $0.8g$. Similarly to E_T in (4), the expectation times for energy recovery increase by a factor of $1/P_S$ if multiple switching attempts are required.

In summary, the reported work has demonstrated the potential of the electrical control mechanism to switch into the HEB of a nonlinear energy harvester within the region of hysteresis. In principle, the control method can be applied to any device with nonlinear hysteresis, having different sizes and transduction methods, through required modifications. The presented physics is generally applicable for other means of a switching mechanism to control the coexisting states of the nonlinear oscillators which may find manifold applications in different branches of science and engineering.

This work is financially supported by Science Foundation Ireland (SFI) Principal Investigator (PI) project on *Vibration Energy Harvesting* Grant No. SFI-11/PI/1201. One of the authors, D. M., is a recipient of the UCC Strategic Research Fund award.

*saibal.roy@tyndall.ie

[1] P. Wang, K. Tanaka, S. Sugiyama, X. Dai, X. Zhao, and J. Liu, Microsyst. Technol. **15**, 941 (2009).
[2] S. Kulkarni, S. Roy, T. O'Donnell, S. Beeby, and J. Tudor, J. Appl. Phys. **99**, 08P511 (2006).
[3] S. P. Beeby, R. N. Torah, M. J. Tudor, P. Glynne-Jones, T. O'Donnell, C. R. Saha, and S. Roy, J. Micromech. Microeng. **17**, 1257 (2007).
[4] S. Roundy and E. Takahashi, Sens. Actuators A **195**, 98 (2013).
[5] M. Han, Q. Yuan, X. Sun, and H. Zhang, J. Microelectromech. Syst. **23**, 204 (2014).
[6] H. Liu, K. H. Koh, and C. Lee, Appl. Phys. Lett. **104**, 053901 (2014).
[7] S. A. Hajati and S.-G. Kim, Appl. Phys. Lett. **99**, 083105 (2011).
[8] G. Gafforelli, A. Corigliano, R. Xu, and S. G. Kim, Appl. Phys. Lett. **105**, 203901 (2014).
[9] D. Mallick, A. Amann, and S. Roy, Smart Mater. Struct. **24**, 015013 (2015).
[10] S. C. Stanton, C. C. McGehee, and B. P. Mann, Appl. Phys. Lett. **95**, 174103 (2009).
[11] F. Cottone, H. Vocca, and L. Gammaitoni, Phys. Rev. Lett. **102**, 080601 (2009).
[12] A. Erturk, J. Hoffmann, and D. J. Inman, Appl. Phys. Lett. **94**, 254102 (2009).
[13] A. F. Arrieta, P. Hagedorn, A. Erturk, and D. J. Inman, Appl. Phys. Lett. **97**, 104102 (2010).
[14] S. Zhou, J. Cao, A. Erturk, and J. Lin, Appl. Phys. Lett. **102**, 173901 (2013).
[15] S. D. Nyugen, E. Halvorsen, and I. Paprotny, Appl. Phys. Lett. **102**, 023904 (2013).
[16] P. Kim and J. Seok, J. Sound Vib. **333**, 5525 (2014).
[17] S. Zhou, J. Cao, D. J. Inman, J. Lin, S. Liu, and Z. Wang, Applied Energy **133**, 33 (2014).
[18] S. Zhou, J. Cao, J. Lin, and Z. Wang, Eur. Phys. J. Appl. Phys. **67**, 30902 (2014).
[19] M. F. Daqaq, R. Masana, A. Erturk, and D. D. Quinn, Appl. Mech. Rev. **66**, 040801 (2014).
[20] L. Tang, Y. Yang, and C. K. Soh, J. Intell. Mater. Syst. Struct. **21**, 1867 (2010).
[21] M. P. Kennedy and L. O. Chua, IEEE Trans. Comput.-Aided Des. Integr. Circuits Syst. **35**, 554 (1988).
[22] D. M. Gvozdic, M. M. Krstic, and J. V. Crnjanski, Opt. Lett. **36**, 4200 (2011).
[23] H. Li, Y. Chen, J. Noh, S. Tadesse, and M. Li, Nat. Commun. **3**, 1091 (2012).
[24] J. Foss, A. Longtin, B. Mensour, and J. Milton, Phys. Rev. Lett. **76**, 708 (1996).
[25] A. N. Pisarchika and U. Feudel, Phys. Rep. **540**, 167 (2014).
[26] B. E. Martinez-Zerega, A. N. Pisarchik, and L. S. Tsimring, Phys. Lett. A **318**, 102 (2003).
[27] L. M. Pecora and T. L. Carroll, Phys. Rev. Lett. **67**, 945 (1991).
[28] W. Yang, M. Ding, and H. Gang, Phys. Rev. Lett. **74**, 3955 (1995).
[29] O. Olusola, U. Vincent, and A. Njah, J. Sound Vib. **329**, 443 (2010).
[30] A. Cammarano, A. Gonzalez-Buelga, S. A. Neild, and S. G. Burrow, J. Phys. Conf. Ser. **476**, 012071 (2013).
[31] S. Zhou, J. Cao, D. J. Inman, S. Liu, W. Wang, and J. Lin, Appl. Phys. Lett. **106**, 093901 (2015).
[32] A. Masuda and T. Sato, Proc. SPIE Int. Soc. Opt. Eng. **9799**, 97990K-1 (2016).
[33] D. A. W. Barton, S. G. Burrow, and L. R. Clare, J. Vib. Acoust. **132**, 021009 (2010).
[34] See Supplemental Material at http://link.aps.org/supplemental/10.1103/PhysRevLett.117.197701 for demonstration of the proposed method for frequency varying, amplitude varying and multi-frequency input vibrations.
[35] E. J. Doedel, R. C. Paffenroth, A. R. Champneys, T. F. Fairgrieve, Y. A. Kuznetsov, B. E. Oldeman, B. Sandstede, and X.-J. Wang, technical report, Department of Computer Science, Concordia University, Montreal, Canada, 2000. Available from http://indy.cs.concordia.ca.